https://doi.org/10.5194/essd-2025-733
Preprint. Discussion started: 10 December 2025

Open Access Earth System Science Data Discussions

A Global 30 m Landsat-based Dataset of Forest Fire Patches (GlobMap FFP v1.0) from 1984 to 2022

Jiaying He[1, †], Xin Zou[1, 2, †], Weihan Zhang[1, 2, †], Quan Duan[1, 2, †], Ronggao Liu[1, *], Yang Liu[1], Jinwei Dong[1], Chaoyang Wu[1], Wei Li[3], Chao Wu[3]

[1]Institute of Geographic Sciences and Natural Resources Research, Chinese Academy of Sciences, Beijing, 100101, China
[2]University of Chinese Academy of Sciences, Beijing, 100101, China
[3]Department of Earth System Science, Ministry of Education Key Laboratory for Earth System Modeling, Institute for Global Change Studies, Tsinghua University, Beijing, 100084, China
[†]These authors contributed equally to this work.

Correspondence to: Ronggao Liu (liurg@igsnrr.ac.cn)

Abstract. Forest fires exert profound ecological impacts globally. Characterizing their long-term effects and evolving regimes requires consistent, high-resolution fire records over extended periods. The Landsat archive provides a unique foundation for such efforts, offering fine spatial detail with globally coherent, multi-decadal observations. Yet, it remains challenging to generate a globally consistent, Landsat-based fire product with event-level characterization. Here we present a 30 m global forest fire patch dataset spanning 1984-2022, developed from the full Landsat archive to ensure comprehensive fire characterization. We first condensed multi-temporal burned signals from Landsat archive on Google Earth Engine (GEE) using a pixel-based image compositing approach. This approach also reduces noise from clouds and shadows while ensuring high computational efficiency using GEE. We then mapped burned area using artificial neural network modeling across global forests. Finally, we delineated individual fire patches through spatial–temporal clustering and extracted their key attributes. Across global forests, we identified a total of 11.97 million individual fire patches burning 7.3 Mha yr^{-1} over 1984 – 2022. Validation indicated omission errors ranging from 12.2% to 36.8% and commission errors ranging from 6.4% to 23.2% across diverse forest types. Intercomparison with existing Landsat products revealed strong agreement in annual burned area estimates and fire patch detection, with discrepancies mainly arising from within-fire delineation and small fire detection. This dataset offers a valuable resource for quantifying fire impacts and advancing the understanding of contemporary and future fire regimes in global forests.

1 Introduction

Forest fires are a major global disturbance with profound ecological impacts on carbon balance, surface energy budget, and ecosystem functioning. Compared with the frequent, lower-intensity burns typical of savannas, grasslands, or croplands, forest fires typically occur less frequently with higher intensity and severity, leading to substantially longer recovery time. As forests store a disproportionate share of terrestrial carbon, these fires consume large amount of woody biomass and soil carbon,

https://doi.org/10.5194/essd-2025-733
Preprint. Discussion started: 10 December 2025

exerting outsized and persistent impacts on global carbon balance (Zheng et al., 2021; Pugh et al., 2019). They also release large quantities of black carbon, aerosols, and volatile organic compounds with tall and long-traveling smoke plumes, generating strong influences on radiation balance, atmospheric chemistry, and regional climate (Liu et al., 2019; Tuccella et al., 2025). Moreover, unlike savannas and grasslands where fire maintains vegetation structure and rapidly cycling biomass, forest fires cause long-lasting alterations in stand structure and species composition, and may even trigger irreversible shifts from closed-canopy forests to shrub- or grass-dominated states (Van Wees et al., 2021; Beck et al., 2011; Brando et al., 2019). In recent decades, climate warming has driven potential shifts in forest fire regimes, including increases in fire frequency, size, severity and recovery time, across diverse forest biomes, reinforcing positive feedbacks that further accelerate climate change (Scholten et al., 2022; Balch et al., 2022; Lv et al., 2025; Iglesias et al., 2022).

Understanding the evolving regimes and impacts of global forest fires requires consistent, high-resolution information of individual fires, such as fire size and frequency, over extended periods. Currently, global burned area products derived from the Moderate Resolution Imaging Spectroradiometer (MODIS) are widely used for large-scale fire patch mapping (Andela et al., 2019; Artés et al., 2019; Balch et al., 2020). Their coarse spatial resolution and relatively short data record constrain analyses of fine-scale spatial patterns and multi-decadal fire dynamics. Landsat's four-decade archive and finer resolution provides a powerful alternative, enabling improved detection of small fires missed by MODIS, precise perimeter delineation for ecological and economic impact assessment, and identification of within-fire ecological refugia essential for biodiversity conservation (Meddens et al., 2016; Ramo et al., 2021; Chuvieco et al., 2019). Yet, global Landsat-based fire monitoring is challenged by high computational demands and cloud-induced data gaps. Most existing products, such as the Burned Area Essential Climate Variable (BAECV) for the conterminous US (CONUS) (Hawbaker et al., 2020) and the Landscape Fire Scars Database (LFSD) for Chile (Miranda et al., 2022), remain regional in scope. Recent global efforts like the Global Annual Burned Area Map (GABAM) (Long et al., 2019) represent important advances but fall short of delivering consistent long-term, patch-scale characterization of forest fires.

Existing algorithms present challenges for using Landsat imagery in globally consistent characterization of forest fires. Burned area mapping methods designed for MODIS are not directly transferable to Landsat because they rely on dense daily observations to capture abrupt spectral changes within short time windows (Chuvieco et al., 2018; Giglio et al., 2018). Landsat's longer revisit interval (~16 days) and the absence of certain spectral bands (e.g., MODIS's 1.24 μm band) preclude these approaches. Time-series detection methods, such as Vegetation Change Tracker (VCT) and LandTrendr, address these limitations for Landsat by identifying abrupt segment changes in multi-year data stacks (Huang et al., 2010; Kennedy et al., 2010). Machine learning-based change detection with annual composites has also been applied for developing burned area products with Landsat, such as GABAM (Long et al., 2019). While effective, such approaches are often computationally intensive for global, multi-decadal analyses due to Landsat's immense data volume. Accurate cloud/shadow detection also remains critical in these methods, as aggressive masking creates data gaps while insufficient clear-sky observations may compromise mosaic quality (Broich et al., 2011). Longer-term image compositing emerged as a strategic solution to mitigate these challenges by generating spatiotemporally consistent, cloud-free composites datasets with condensed disturbance signals

https://doi.org/10.5194/essd-2025-733
Preprint. Discussion started: 10 December 2025

while substantially reducing data volume, making global-scale monitoring feasible (Francini et al., 2023; Qiu et al., 2023). The choice of compositing criterion involves critical trade-offs in detection accuracy, efficiency, and sensitivity to noise (Miettinen and Liew, 2008; Otón et al., 2019; Hermosilla et al., 2019; Senf and Seidl, 2021a). For example, the best available pixel (BAP) method produces high-quality mosaics but with increased computational cost (White et al., 2014). The minimum NIR method is highly effective for burned area detection but is sensitive to cloud shadows, requiring additional processing (Miettinen and Liew, 2008; Chuvieco et al., 2005).

In this study, we present GlobMap Forest Fire Patches (GlobMap FFP) v1.0 (Liu, 2025), a 30 m dataset mapping individual fire patches in global forests from 1984 to 2022 utilizing the full Landsat archive. We first applied a multi-temporal, pixel-based image compositing approach on the Google Earth Engine (GEE) platform to condense spectral signals of forest fires while reducing contamination from clouds and shadows, leveraging both the extensive Landsat archive and GEE's computational capacity. We then mapped burned area in global forests using artificial neural network (ANN) models trained for various forest types. We further delineated and encoded individual fire patches using a spatiotemporal clustering algorithm based on spatial proximity and year of occurrence, constrained by Landsat's revisit cycle. Each fire patch is assigned with a unique ID along with its patch size and burned year. Finally, we evaluated the performance of the dataset through independent validation and intercomparison with existing products.

2 Datasets

2.1 Landsat imagery

Landsat satellites provide continuous, high-resolution, multi-spectral observations of Earth's surface at a global scale. Their optical sensors capture imagery across visible, infrared, and thermal wavelengths, with a swath width of 185 km and a 16-day revisit cycle. For this study, we used Level-2 surface reflectance data from all available Landsat imagery archived on the GEE platform from 1984 to 2022. We considered data from Landsat 5 Thematic Mapper (TM; 1984 – 2013), Landsat 7 Enhanced Thematic Mapper Plus (ETM+; 1999 – 2021), and Landsat 8 Operational Land Imager (OLI; 2013 – 2022), which all share similar band configurations. Surface reflectance data from Landsat 5 TM and Landsat 7 ETM+ were processed using the Landsat Ecosystem Disturbance Adaptive Processing System (LEDAPS) algorithm, while data from Landsat 8 and 9 OLI were generated using the Land Surface Reflectance Code (LaSRC). We focused on the green, red, near infrared (NIR), and long shortwave infrared (SWIR) bands and their derived vegetation indices for product development.

2.2 Auxiliary datasets

We generated a global forest mask for extracting forest fires using MODIS-based tree cover and land cover products. Tree cover was derived from the 250 m global annual tree cover product (GLOBMAP FTC; https://doi.org/10.5281/zenodo.10589730), which improves global tree cover estimates by leveraging highly discriminative spectral features and extensive near-global training samples (Liu et al., 2024). We first constructed a maximum tree cover layer

https://doi.org/10.5194/essd-2025-733
Preprint. Discussion started: 10 December 2025

by selecting the highest tree cover value for each pixel during 2000–2021. We then defined forests as areas with the derived maximum tree cover larger than 25%. We further excluded tropical savannas and shrublands using the MODIS land cover product MCD12Q1 under the International Geosphere-Biosphere Programme (IGBP) classification scheme (Sulla-Menashe et al., 2019). This product was chosen for its ability to effectively distinguish savannas and shrublands from forested areas in the tropics.

Additionally, we used the MODIS burned area product MCD64A1 (Giglio et al., 2018) over 2001-2022 as a reference to generate Landsat-based training samples for ANN modeling of global forest burned area. The MCD64A1 product provides monthly burned area information at a 500 m resolution based on changes from both surface reflectance and thermal anomalies. We also incorporated the 30 m Global Forest Change (Hansen et al., 2013) and Global Forest Losses due to Fire (Tyukavina et al., 2022) products (https://glad.umd.edu/dataset) to generate samples for capturing non-fire disturbances such as logging, ensuring comprehensive fire scar characterization.

2.3 Intercomparison datasets

Existing fire datasets with comparable spatial resolutions were employed for intercomparison to assess the performance of our product at both regional and global scales (Table 1). We considered four Landsat-based burned area products for regional comparison: the BAECV (https://doi.org/10.5066/P9QKHKTQ) for the CONUS, the European Forest Disturbance Maps (EFDM; https://doi.org/10.5281/zenodo.3924381) for Europe, the LFSD https://doi.org/10.1594/PANGAEA.941127) for Chile, and the MapBiomas Fire Collection (https://brasil.mapbiomas.org/en/mapbiomas-fogo/) for Brazil. The BAECV product, developed by the US Geological Survey, maps annual burned area across the CONUS from 1984 onward using dense Landsat time-series (Hawbaker et al., 2020). In Europe, the EFDM provides 30 m annual maps of forest disturbances and distinguishes fire-driven and storm-driven records during 1986 – 2021 (Senf and Seidl, 2021b, a). The LFSD provides detailed records on burned area, fire size, perimeter, and severity for individual fires in Chile from 1985 to 2018 (Miranda et al., 2022). The MapBiomas Fire Collection characterizes long-term fire dynamics in Brazil since 1985 (Alencar et al., 2022). Globally, we used the MODIS-based burned area product MCD64A1 for intercomparison (Giglio et al., 2018). This widely used product provides monthly 500 m burned area maps from 2000 onward, derived using a hybrid algorithm that integrates thermal anomalies, surface reflectance, and contextual information to detect burn scars.

3 Methods

The development of the GlobMap FFP product involved three main steps (Fig. 1). First, we applied a pixel-based image compositing algorithm to generate multi-year Landsat composites at approximately five-year intervals. Second, we mapped burned area pixels using spectral information from the composites with ANN regression modeling. We further applied a spatiotemporal clustering algorithm to segment the mapped burned area pixels from the previous step into distinct fire scars, and encoded each as an individual fire patch. The image compositing step was conducted on the GEE platform, while the

https://doi.org/10.5194/essd-2025-733
Preprint. Discussion started: 10 December 2025

Open Access Earth System Science Data Discussions

subsequent burned area mapping and fire patch segmentation processes were performed offline on a local computing server. Finally, the product was evaluated through validation and intercomparison against existing products.

Table 1: List of fire products adopted for intercomparison

Products	Regions	Sensors	Periods	Spatial resolutions	Temporal resolutions	References
MCD64A1	Global	MODIS	2001-2021	500 m	Monthly	(Giglio et al., 2018)
Burned Area Essential Climate Variable (BAECV)	CONUS	Landsat	1984-2021	30 m	Annual	(Hawbaker et al., 2020)
European Forest Disturbance Map (EFDM)	Europe	Landsat	1986-2016	30 m	Annual	(Senf and Seidl, 2021b, a)
MapBiomas Fire Collection	Brazil	Landsat	1985-2020	30 m	Annual	(Alencar et al., 2022)
Landscape Fire Scars Database (LFSD)	Chile	Landsat	1985-2018	30 m	Monthly	(Miranda et al., 2022)

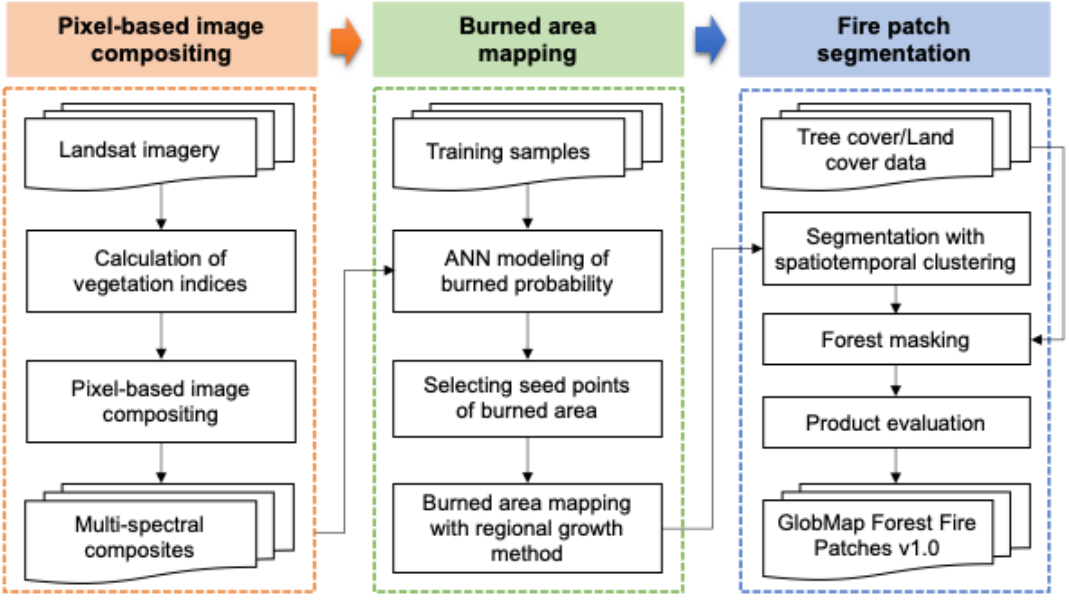

Figure 1: Overall workflow for developing the 30 m GlobMap Forest Fire Patches v1.0 product.

https://doi.org/10.5194/essd-2025-733
Preprint. Discussion started: 10 December 2025

Open Access Earth System Science Data Discussions

3.1 Product development

3.1.1 Pixel-based image compositing

We generated multi-year composites by condensing Landsat time-series imagery into five-year periods and retaining the strongest spectral signals of burned vegetation within each interval. Due to the limited availability of clear-sky imagery before 2000, the pre-2000 data were grouped into two longer compositing periods: 1984 – 1990 and 1991 – 2000. For the post-2000 era, imagery was composited at regular five-year intervals: 2001 – 2005, 2006 – 2010, 2011 –2015, 2016 – 2020, and 2021 – 2022. For each interval, the compositing layers were generated using all available Landsat observations from all sensors operating during that period.

Here we employed the minimum Brown Vegetation Index (BVI) compositing approach (Liu, 2017) to generated multi-year imagery. While minimum NIR or NDVI compositing is widely adopted for burned area mapping, using these indices alone is sensitive to contamination like clouds, aerosols, shadows, and water bodies, and can be compromised by imperfect cloud and shadow masking (Chuvieco et al., 2005; Miettinen and Liew, 2008; Barbosa et al., 1998). Overly aggressive masking further reduces the availability of high-quality Landsat observations in cloud-prone regions (Broich et al., 2011). The BVI approach mitigates these issues by exploiting it distinct spectral response to vegetation disturbance and atmospheric contamination. Calculated as a normalized ratio between the green and SWIR at 2.1 μm (SWIR2) bands (Liu, 2017), BVI effectively separates burned signals from confounding factors due to its contrasting sensitivity: SWIR2 reflectance increases markedly after fire due to moisture reduction and charcoal deposition, while green reflectance decreases with vegetation damage (Chuvieco et al., 2019). This produces a characteristically low BVI value, distinct from both atmospheric contaminants and seasonal senescence. In contrast, healthy vegetation, clouds, snow, and shadows elevate BVI.

For each pixel, we first identified ten candidate observations with the lowest BVI values using Landsat time series within each compositing interval. Among these candidates, the observation with the lowest surface reflectance in the NIR band was selected to generate the compositing layer. The acquisition year of the retained observation was recorded as the burned year. The final compositing layer incorporates all Landsat surface reflectance bands, as well as the burned year. This approach can reliably capture post-fire conditions even in regions with frequent cloud cover or short post-fire visibility windows (Fig. 2). Compared with annual compositing, this multi-year compositing method reduces the substantial computational burden of processing global-scale Landsat data on GEE, and effectively prevents repeated detection in severely burned scars that persist for years in remote sensing imagery.

https://doi.org/10.5194/essd-2025-733
Preprint. Discussion started: 10 December 2025

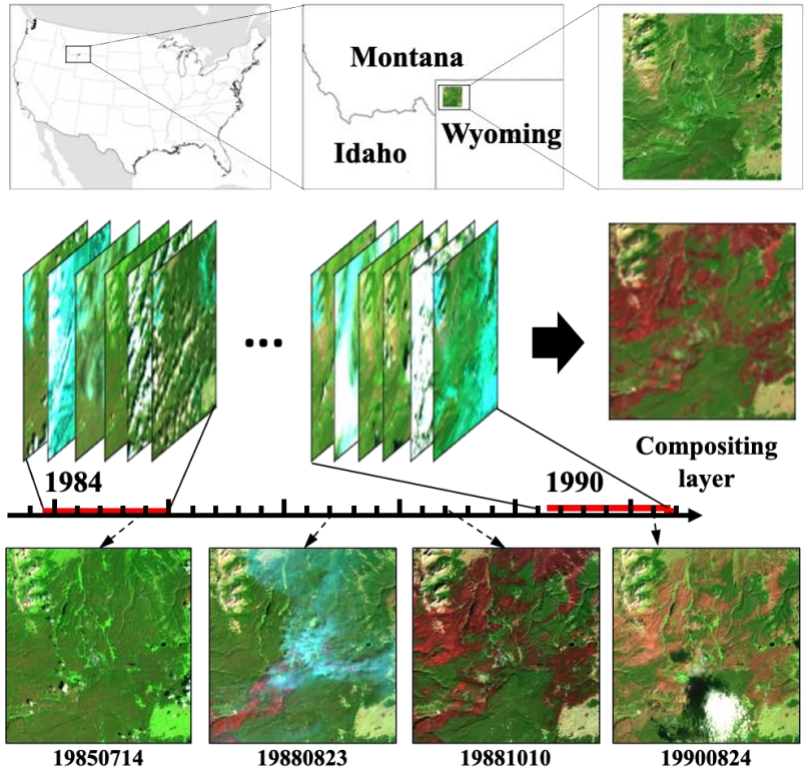

Figure 2. Illustration of the multi-year compositing procedure for deriving the compositing layer with condensed burned signals, shown here using Landsat imagery from 1984–1990 in Yellowstone National Park as an example.

3.1.2 Burned area mapping

Training samples of burned and unburned pixels were derived from Landsat imagery using the MCD64A1 burned area and MCD12Q1 land cover products as a spatial reference. We first divided the globe into 2°×2° grid cells and overlaid each grid with Landsat Thiessen Scene Area (TSA) units, together with MCD12Q1 and MCD64A1 data over 2001 – 2022. For each grid, we selected Landsat tiles with forest cover exceeding 80% and the largest burned area, yielding a total of 800 tiles for sample extraction. Burned pixels within each tile were then delineated using a maximum curvature segmentation method (Duan et al., 2024), which adaptively determines thresholds based on SWIR2 and NIR reflectance changes to efficiently detect burned surfaces from single-date image. All segmentation outputs were visually inspected to ensure mapping quality. Burned samples were then randomly drawn from these detected burned pixels, while unburned samples were taken from nearby unaffected forest pixels. Because Landsat composites may include non-fire disturbances (e.g., logging), we also collected samples of non-fire forest loss and treated them as unburned to help the model distinguish fire from other disturbance types. Specifically, we separated fire-related forest loss identified in the Global Forest Loss due to Fire dataset (Tyukavina et al., 2022) from all forest loss in the 30 m Global Forest Change product (Hansen et al., 2013), and used the remaining loss as non-fire disturbance.

https://doi.org/10.5194/essd-2025-733
Preprint. Discussion started: 10 December 2025


Open Access Earth System Science Data Discussions

We then developed an ANN regression model to estimate the burned probability of each pixel. We extracted the surface reflectance values of the samples from all Landsat bands in the multi-year composites and calculated vegetation indices including NBR, NDVI, and normalized different wetness index (NDWI). These metrics were employed as input features for developing the ANN model. The model included five hidden layers with 500, 400, 200, 100, and 50 neurons respectively, using the ReLU activation function (Nair and Hinton, 2010). The output layer contained a single neuron with a sigmoid activation function, yielding a burned area probability ranging from 0 to 1. Next, for burned area mapping, we identified seed points with burn probabilities higher than 80%. A regional growing algorithm was then applied to expand the seed points and delineate the full extent of the burned area. Pixels with burn probabilities greater than 40% and located within an 8-connected neighborhood were further aggregated into the final burned area.

3.1.3 Fire patch segmentation

Here we considered burned area pixels within a distance of 20 Landsat pixels and occurred in the same year as a single fire patch, and encoded them with a certain fire ID. Temporal segmentation relied solely on burned year, constrained by the inconsistency of cloud-free Landsat observations, which limits more precise temporal delineation. For each fire patch, we assessed the uncertainty of burned area detection by comparing its spectral signals to those of the surrounding reference pixels. Burned scars typically have lower surface reflectance in NIR band, a greater difference between the SWIR2 and NIR bands ($\rho_{SWIR2} - \rho_{NIR}$), and a greater difference between the SWIR2 and Red bands ($\rho_{SWIR2} - \rho_{Red}$), compared to undisturbed reference pixels. The reference pixels were extracted from the 10-pixel outer border of each fire patch with a pre-burning land cover type of forests. Training samples generated in **Section 3.1.2** were reused here to estimate the probability of uncertainty through ANN modeling. We constructed an ANN model using surface reflectance from the Red, NIR, SWIR2 bands, as well as the differences between SWIR2 and NIR bands and between SWIR2 and Red bands, as input features. Based on the probability of uncertainty, we categorized the detected fire patches into four QA levels: level 1 (75 – 100%), level 2 (50 – 75%), level 3 (25 – 50%), and level 4 (0 – 25%). Here Level 1 indicates the highest confidence in detecting a fire patch, while level 4 indicates the lowest.

Furthermore, we filtered out non-forest fire patches and excluded potential logging sites from the identified burned scars. Fire patches were removed if more than 50% of their pixels were located outside the forest extent, based on a forest mask derived from MODIS-based GLOBMAP fractional tree cover and MCD12Q1 land cover products. Potential logging patches were then excluded from burned patches by analyzing their geometric characteristics, as they typically have regular shapes and smooth edges. Specifically, we calculated fractal dimension and perimeter-area ratio for each patch. Additionally, fire patches smaller than 20 Landsat pixels (1.8 ha) were excluded to reduce detection uncertainties. The final dataset provides detailed records of individual fire patches at a 30 m resolution.

https://doi.org/10.5194/essd-2025-733
Preprint. Discussion started: 10 December 2025

3.2 Product evaluation

3.2.1 Validation

We referred to the sample selection criteria of the burned area reference database (BARD) and independently constructed reference data from Landsat imagery for product validation. The BARD product utilizes a systematic sampling strategy and manual visual interpretation to provide high-quality reference data (Franquesa et al., 2020). In total, we sampled 74 Landsat TSA units across various forest (Fig. 3). All Landsat images with cloud cover below 40% were downloaded for each selected TSA unit, resulting in a total of 945 tiles. For each sampled Landsat scene, we independently mapped the burned area in forests as a reference dataset, using the same algorithm we adopted for generating training samples (Duan et al., 2024). The detection results for each scene were then composited to generate burned area reference samples for the corresponding Landsat TSA unit. Next, we derived the confusion matrix and calculated the accuracy metrics for five forest types defined by MODIS land cover data, including commission error (CE), omission error (OE), Dice coefficient (DC), and relative bias (relB), to quantify the performance of the product (Padilla et al., 2015).

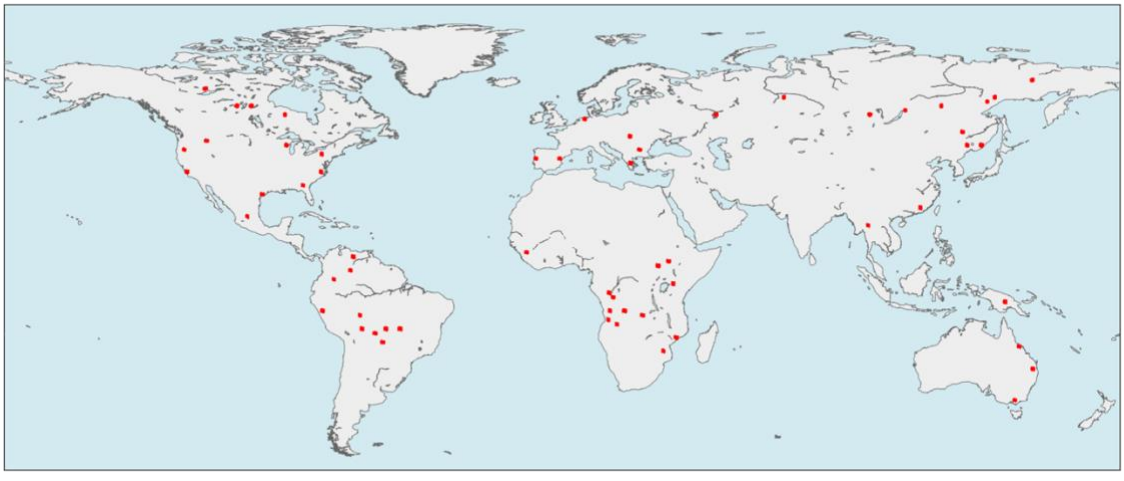

Figure 3. Spatial coverage of sampled Landsat Thiessen Scene Area (TSA) units for validation.

3.2.2 Product intercomparison

We conducted intercomparisons between our dataset and established global and regional burned area products to assess their spatial and temporal consistency. At the global scale, we compared GlobMap with the MODIS-based MCD64A1 product across all fourteen Global Fire Emission Dataset (GFED) regions, focusing on the post-2001 period to match MCD64A1's temporal coverage. Regionally, we analyzed four Landsat-based products with long-term data availability since the 1980s (Table 1): BAECV for the CONUS, LFSD for Chile, EFDM for Europe, and MapBiomas Fire for Brazil. forest burned area was extracted from all products using the method described in **Section 3.1.3** to ensure comparability.

We performed three types of intercomparisons: temporal trend, spatial agreement, and temporal agreement. First, we assessed annual time series of forest burned area to evaluate how well GlobMap captures fire patterns relative to other datasets. At the

https://doi.org/10.5194/essd-2025-733
Preprint. Discussion started: 10 December 2025

regional level, we performed three sets of pairwise comparisons across the four regions (CONUS, Chile, Europe, and Brazil): (1) GlobMap vs. MCD64A1; (2) Landsat-based products (BAECV, LFSD, EFDM, and MapBiomas) vs. MCD64A1; (3) GlobMap vs. Landsat-based products. At the global scale, we compared GlobMap and MCD64A1 products across the fourteen GFED regions. For each product pair, we calculated annual forest burned area and evaluated their relationships using linear regression and Pearson's correlation coefficient.

Second, we evaluated the spatial agreement of individual fire patches across products to better understand the sources of discrepancies in burned area detection. Using the method described in **Section 3.1.3**, we identified annual fire patches in MCD64A1 and the four regional products, then performed one-to-one matching of fire patches across the same three sets of regional comparisons, as well as a global comparison between GlobMap and MCD64A1. For each product pair, we classified the burned pixels into five groups (Fig. 4): (1) No overlap – unique to Product 1, (2) Overlap – detected only by Product 1, (3) Overlap – detected by both products, (4) Overlap – detected only by Product 2 only, and (5) No overlap – unique to Product 2. Groups 1 and 5 represent unmatched fire patches unique to each product. Groups 2 and 4 indicate partial spatial agreement (shared patches but divergent extents), and Group 3 reflects full agreement in fire extent. We then quantified the proportion of each group relative to the total burned area across both products to assess the degree of spatial agreement. Specifically, we summarized three agreement levels: (1) Full agreement - Group 3; (2) Partial agreement - Groups 2 and 4; (3) Disagreement - Groups 1 and 5. We further stratified the analysis by fire size, summarizing group-level results separately for smaller (< 200 ha) and larger (> 200 ha) fire patches.

Third, we assessed temporal agreement by examining differences in fire detection year between the GlobMap and the other products. For each comparison, we randomly sampled 30% of the burned pixels identified by both products and calculated the fraction with burned year discrepancies within a ±3-year window (Senf and Seidl, 2021a). Consistent with the spatial analysis, we stratified the results by fire size to evaluate the influence of patch magnitude on temporal consistency.

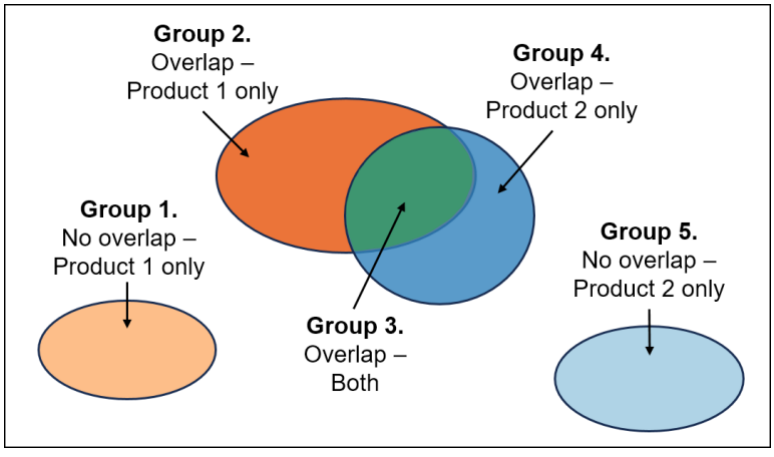

Figure 4. Conceptual framework of the spatial agreement analysis based on one-to-one matching of individual fire patches between two products. Groups 1 and 5 represent unmatched fire patches unique to each product, while groups 2 and 4 reflect burned pixels detected only by one product within matched patches. Group 3 includes pixels jointly detected by both products.

https://doi.org/10.5194/essd-2025-733
Preprint. Discussion started: 10 December 2025

4 Results

4.1 Distribution of global forest fires

Between 1984 and 2022, we identified a total of 11.97 million individual fire patches across global forests based on the newly developed dataset from this study. We further summarized the spatial distributions and annual time series of burned area, fire occurrences, and mean fire size associated with the identified fire patches globally. Burned area shows diverse spatial distribution patterns across global forests (Fig. 5a). Larger burned area is concentrated in the boreal forests of North America and Eurasia, as well as in the tropical forests of South America and South Asia. Specifically, boreal forests in North America and Eurasia, as defined by the Köppen−Geiger Climate Classification (Beck et al., 2023), accounted for 60.0% of the total burned area in global forests over the past four decades. Nevertheless, the underlying mechanisms driving the spatial distributions of the burned area are different: boreal forests typically experience less frequent but more extensive fire patches, whereas tropical forests are characterized by smaller but more frequent burnings (Fig. 5b-c).

Unlike burned area, occurrences of individual fires in global forests exhibit distinct spatial patterns across latitudes (Fig. 5b). Over the past four decades, tropical forests in regions such as South America, Africa, and South Asia, have experienced a substantially higher fire occurrences compared to forests in temperate or boreal ecoregions. These elevated fire occurrences are often associated forests with anthropogenic fire use activities, such as deforestation and fuel management practices (Archibald et al., 2013). For example, in North America, forests in southeastern US, where human activities are the primary cause of fire ignitions, have experienced higher fire frequency than the boreal forests, where fires are predominately triggered by lightning (Veraverbeke et al., 2017). Compared to fire occurrences, mean fire size shows contrasting distribution patterns across latitudes in global forests (Fig. 5c). More extended fire patches are predominantly observed in temperate and boreal forests at high northern latitudes, whereas temperate and tropical forests in lower latitudes are characterized by smaller-scale burnings. This spatial variation aligns with MODIS-based findings on fire size across global land cover types (Hantson et al., 2015). These differences are likely driven by a combination of climate factors, including gradients of precipitation and aridity, as well as the influence of human activities.

https://doi.org/10.5194/essd-2025-733
Preprint. Discussion started: 10 December 2025

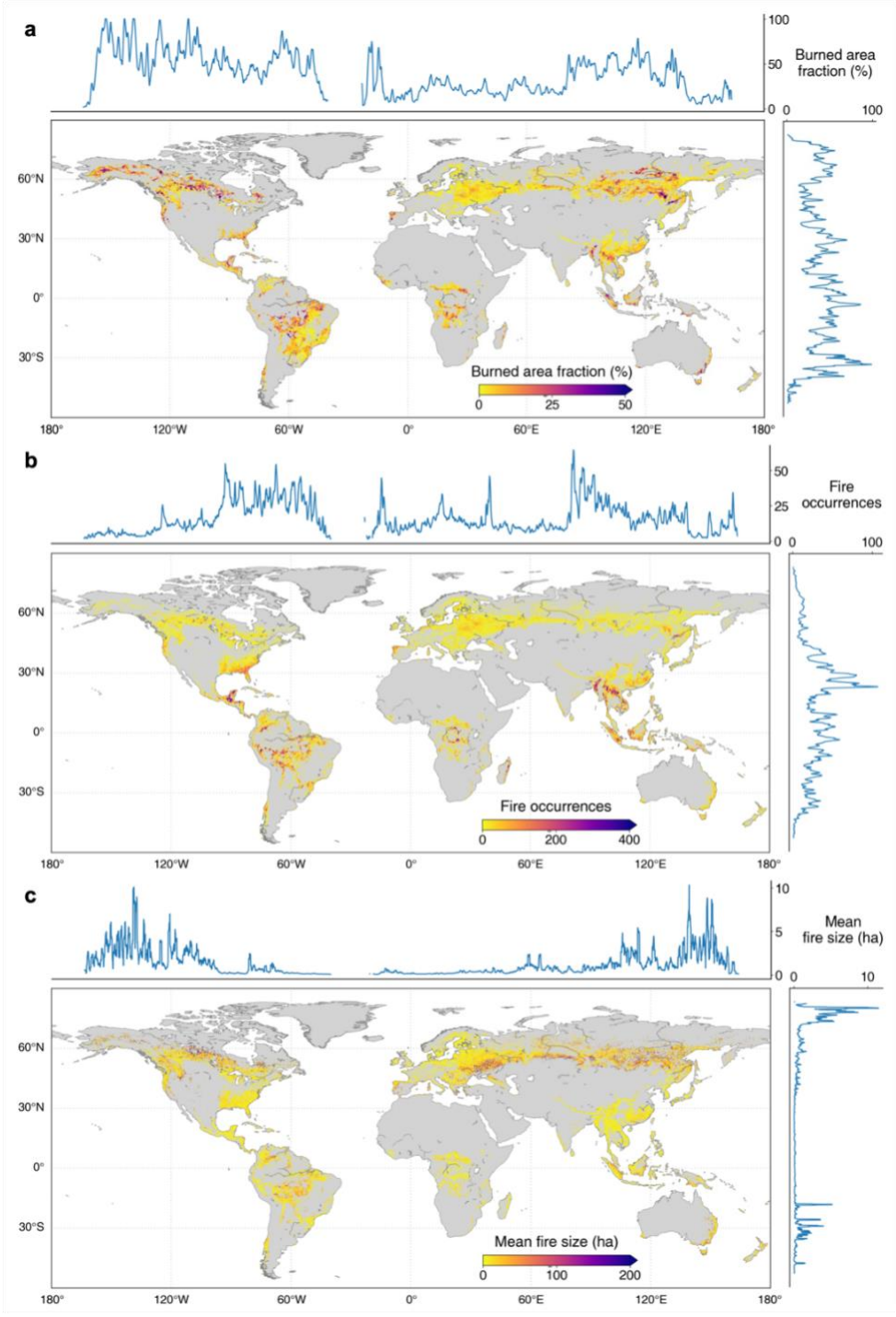

Figure 5. Spatial distributions of total global forest fires over 1984 – 2022 based on the dataset developed in this study. (a) Burned area fraction (%), (b) fire occurrences, (c) mean fire size (ha). The variables were aggregated at a 0.1° resolution for data visualization.

https://doi.org/10.5194/essd-2025-733
Preprint. Discussion started: 10 December 2025

4.2 Validation

Across global forests, the GlobMap product showed a Dice Coefficient of 0.82, with a commission error (CE) rate of 23.8% and an omission error (OE) rate of 13.2% for detecting forest burned area at a global scale (Table 3). Omission and commission error rates were more variable across different forest types. The omission error rates ranged from 12.2% to 36.8%, with the lowest in evergreen needleleaf forests, and the highest in mixed forests. The commission error rates ranged from 6.4% to 23.2%, with the lowest in evergreen needleleaf forests and the highest in deciduous broadleaf forests. Overall, detected forest burned area generally had relatively higher OE and slightly lower CE rates.

Table 2. Summary of validation results across various forest types.

Forest types	Dice Coefficient (DC)	Omission Error (OE)	Commission Error (CE)	Relative Bias (relB)
Evergreen needleleaf	0.91	0.12	0.06	-0.07
Deciduous needleleaf	0.86	0.18	0.10	-0.09
Deciduous broadleaf	0.75	0.30	0.23	-0.08
Evergreen broadleaf	0.71	0.37	0.19	-0.23
Mixed	0.80	0.26	0.12	-0.16
Total	0.82	0.24	0.13	-0.11

4.3 Product intercomparison

4.3.1 Annual burned area in forests

Comparisons between GlobMap and existing products generally showed consistent estimates of annual forest burned area at the regional scale. GlobMap exhibited strong very linear relationships ($p < 0.01$, $R^2 > 0.5$, $r > 0.75$) with the regional products, except in Europe (Fig. 6). It estimated higher annual burned area than LFSD in Chile, but lower values than BAECV in CONUS and MapBiomas in Brazil. Over the past four decades, the mean annual burned area in Chilean forests detected by GlobMap was about 2.43 times that of LFSD. In CONUS, BAECV reported a mean annual burned area of 0.52 Mha year^{-1}, 1.69 times that of GlobMap (0.31 Mha year^{-1}) (Table 4). Similarly, in Brazil, MapBiomas estimated annual forest burned area about 1.58 times that of GlobMap. GlobMap also showed moderate agreement with MCD64A1 in CONUS, Chile, and Brazil ($p < 0.1$). Nevertheless, all three products exhibited weak agreement in European forests. For example, a negative correlation ($r = -0.36$) was found between GlobMap and EFDM. This discrepancy is likely caused by methodological differences: while other products directly map burned area based on spectral changes, EFDM first identifies all forest disturbances and then distinguishes fire- from storm-driven events using a machine learning-based attribution model (Senf and Seidl, 2021b, a).

A global comparison between GlobMap and MCD64A1 reveals regional variability in annual forest burned area. From 2001 to 2021, GlobMap (7.3 Mha yr^{-1}) estimated a lower average of global annual burned area than MCD64A1 (19.59 Mha yr^{-1}) in

https://doi.org/10.5194/essd-2025-733
Preprint. Discussion started: 10 December 2025

global forests, largely due to underestimation in tropical regions (Fig. 7). In boreal and temperate domains, including BONA, TENA, EURO, EQAS, and BOAS, the two products showed broadly comparable burned area estimates over the past two decades, with significant linear relationships ($p < 0.1$) observed between their annual values. Across most tropical forests in NHSA, NHAF, SHAF, and SEAS, MCD64A1 reported substantially higher annual burned area than GlobMap. This systematic divergence reflects differences in both spatial and temporal resolutions of the two products. The coarse MODIS pixel size can lead to higher burned area estimates than Landsat, as saturated infrared responses from subpixel fires may cause an entire pixel to be labeled as burned (Robinson, 1991). The daily MODIS observations also enable detection of short-lived surface fires that rapidly fade as understory vegetation regrows in tropical forests. By comparison, the sparse clear-sky temporal coverage of Landsat limits the capability to capture such transient burns in cloud-prone tropical regions (Roteta et al., 2019). Additionally, the multi-year compositing approach used in GlobMap may underestimate burned area associated with frequent, low-intensity surface fires that primarily affect understory fuels.

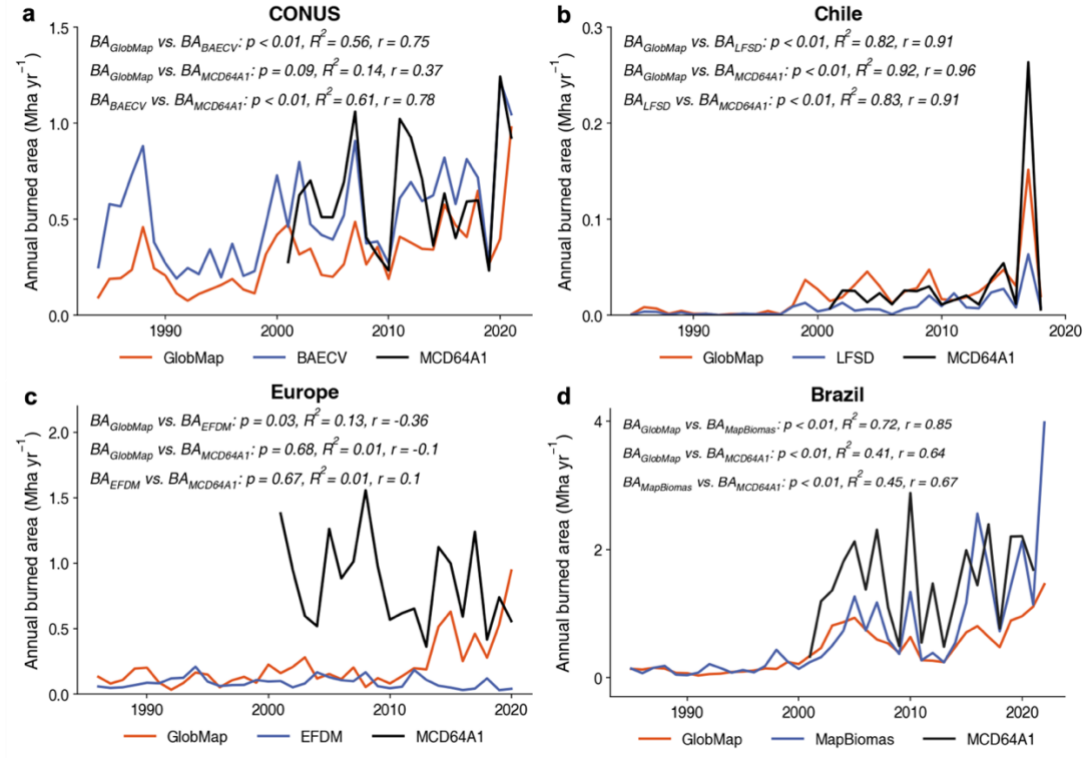

Figure 6. Comparison of annual forest burned area estimates from Landsat-based products (GlobMap and four regional datasets) and MCD64A1 across four regions over the past decades. (a) CONUS: GlobMap, BAECV, and MCD64A1 (1984 – 2021). (b) Chile: GlobMap, LFSD, and MCD64A1 (1985 – 2018). (c) Europe: GlobMap, EFDM, and MCD64A1 (1986 – 2020). (d) Brazil: GlobMap, MapBiomas, and MCD64A1 (1985 – 2022). GlobMap is represented in orange, the four regional products (BAECV, LFSD, EFDM, and MapBiomas) in purple, and MCD64A1 in black. Each subplot includes linear regression statistics and Pearson's correlation coefficients between annual burned area estimates from each product pair.

Table 3. Annual forest burned area in four regions from Landsat-based and MCD64A1 products.

https://doi.org/10.5194/essd-2025-733
Preprint. Discussion started: 10 December 2025

Periods	Products	Annual forest burned area (Mha yr^{-1})			
		CONUS	Chile	Europe	Brazil
1980s – 2020s	GlobMap	0.308	0.021	0.213	0.431
	Regional products	0.522	0.009	0.088	0.680
2001 – 2020s	GlobMap	0.396	0.034	0.281	0.624
	Regional products	0.618	0.014	0.086	0.930
	MCD64A1	0.617	0.034	0.849	1.492

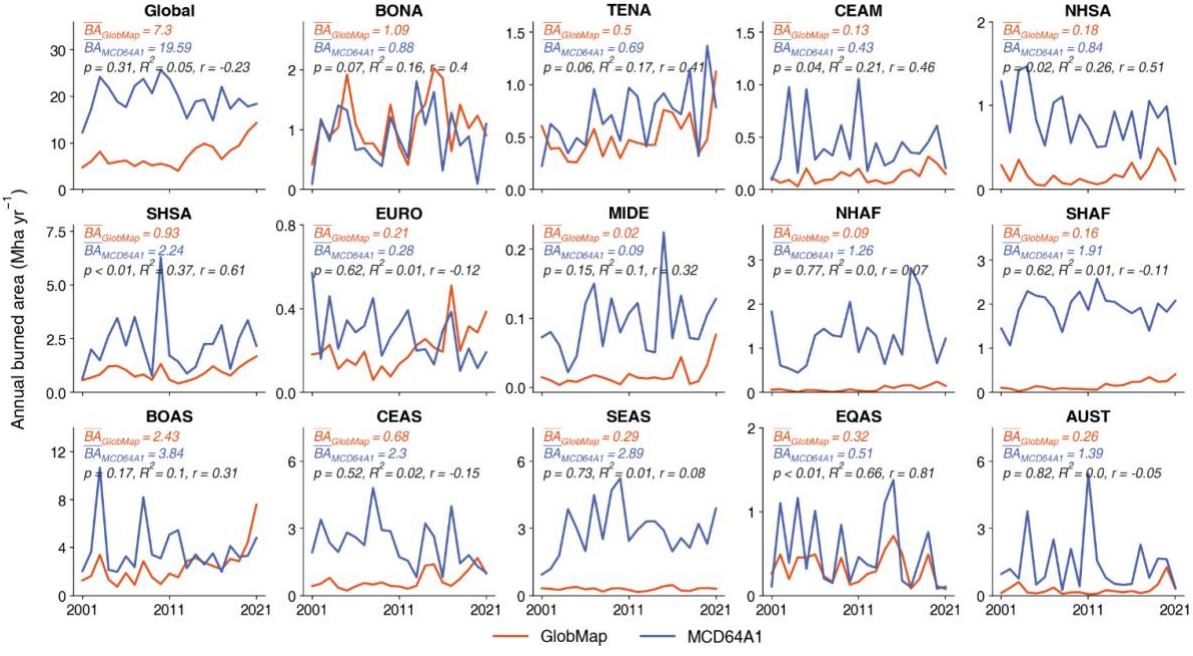

Figure 7. Comparison of annual burned area in global forests derived from the GlobMap and MCD64A1 products from 2001 to 2021. The burned area is summarized for both global forests and forests in the fourteen GFED regions. Results from GlobMap and MCD64A1 are represented in orange and purple colors, respectively. Their annual averages of forest burned area are displayed in each subplot. Relationships between annual forest burned area from the two products, derived from linear regression and Pearson's r correlation, are also denoted in each subplot.

4.3.2 Spatial agreement of fire patches

Regional comparisons demonstrated strong spatial consistency between GlobMap and other Landsat-based products, with high levels of full or partial spatial agreement, especially for larger fires (Fig. 8a; Table 5a). In Chile, Brazil, and Europe, 93.2%, 95.0%, and 86.7% of the burned area from GlobMap, respectively, overlapped with regional products. In particular, over 65% of the burned area in Chile and Brazil exhibited full spatial agreement, indicating strong spatial alignment in fire extent detection. Agreement in the CONUS was more moderate with 74.2% of the burned area showing full or partial overlap, largely due to BAECV mapping substantially more extensive burned area within the same fire patches. This is reflected in BAECV's

https://doi.org/10.5194/essd-2025-733
Preprint. Discussion started: 10 December 2025

high proportion of Group 4 burned area and is consistent with its higher annual burned-area estimates. Despite this overall consistency, differences in within-fire patch delineation and the ability to detect small fires contribute to discrepancies in mapping results. Across all regions, GlobMap detected more smaller fires than the regional products, as evidenced by the higher burned area fractions in Group 1 compared to Group 5. In particular, for smaller fires, approximately 50.2% and 47.2% of the burned area in Europe and Chile were uniquely detected by GlobMap. These results suggest that differences in small fire detection capability are another contributor to inconsistencies among burned area products.

Comparisons between the Landsat- and MODIS-based products revealed consistently high levels of partial spatial agreement in burned area detection for both GlobMap and the four regional products. In the comparison between GlobMap and MCD64A1, the largest share of burned area fell into Group 4, fire patches shared by both products but with additional burned pixels mapped only by MCD64A1 (Fig. 8b). This likely reflects differences in within-patch delineation for overlapping fires, a pattern that was consistent across all four regions and both fire-size classes. Specifically, Group 4 comprised more than 47.6% of the burned area for smaller fires and 43.8% for larger ones (Fig. 8b). GlobMap, by contrast, detected more burned area from small fires than MCD64A1 (Group 1), highlighting the benefit of higher spatial resolution for capturing fine-scale burns. When compared to GlobMap, the four regional products tended to omit a greater portion of burned area uniquely detected by MCD64A1 (Group 5) (Fig. 8b-c).

At the global scale, GlobMap and MCD64A1 exhibited relatively high partial spatial agreement, consistent with the regional comparisons (Fig. 9). For larger fires, most discrepancies arose from two systematic patterns: MODIS tended to map more extensive burned area within matched fire patches (Group 4) and to detect additional fires (Group 5) in tropical forests (e.g., NHSA, NHAF, and SHAF) compared with GlobMap. These differences likely suggest that the high temporal frequency of the MODIS sensors enables more continuous tracking of fast-spreading surface fires or burns that recover rapidly, especially in the cloud-prone tropical regions where Landsat's lower temporal resolution limits observation opportunities. For smaller fires, the sources of disagreement differed. MCD64A1 consistently mapped larger burned extents for matched patches (Group 4). GlobMap also identified more small fires not captured by MCD64A1 (Group 1), especially in regions like TENA and EURO. This underscores the advantage of Landsat's finer spatial resolution for detecting small-scale forest fires.

https://doi.org/10.5194/essd-2025-733
Preprint. Discussion started: 10 December 2025

Open Access Earth System Science Data Discussions

Table 4. Statistical summary of spatial agreement levels from regional comparisons

(a) GlobMap vs. Regional products				
Regions	**Fire size groups**	**Full agreement (Group 3)**	**Partial agreement (Groups 2 + 4)**	**Disagreement (Groups 1 +5)**
CONUS	Smaller	22.5%	65.1%	12.4%
	Larger	28.1%	46.1%	25.8%
Chile	Smaller	15.4%	35.7%	48.9%
	Larger	65.7%	27.5%	6.8%
Europe	Smaller	4.3%	37.6%	58.2%
	Larger	24.4%	62.5%	13.1%
Brazil	Smaller	51.4%	31.8%	16.8%
	Larger	65.5%	29.5%	5.0%
(b) GlobMap vs. MCD64A1				
Regions	**Fire size groups**	**Full agreement (Group 3)**	**Partial agreement (Groups 2 + 4)**	**Disagreement (Groups 1 +5)**
CONUS	Smaller	5.8%	61.5%	32.7%
	Larger	28.6%	59.5%	11.9%
Chile	Smaller	9.5%	57.5%	33.0%
	Larger	44.1%	47.0%	8.9%
Europe	Smaller	9.2%	54.4%	36.4%
	Larger	30.0%	63.2%	6.8%
Brazil	Smaller	25.4%	55.3%	19.3%
	Larger	37.5%	57.3%	5.2%
(c) Regional products vs. MCD64A1				
Regions	**Fire size groups**	**Full agreement (Group 3)**	**Partial agreement (Groups 2 + 4)**	**Disagreement (Groups 1 +5)**
CONUS	Smaller	4.2%	65.1%	30.7%
	Larger	22.0%	47.7%	30.3%
Chile	Smaller	2.8%	75.8%	21.4%
	Larger	31.0%	41.9%	27.1%
Europe	Smaller	4.2%	74.4%	21.4%
	Larger	10.2%	39.4%	50.4%
Brazil	Smaller	21.4%	50.6%	28.0%
	Larger	48.1%	28.4%	23.5%

https://doi.org/10.5194/essd-2025-733
Preprint. Discussion started: 10 December 2025

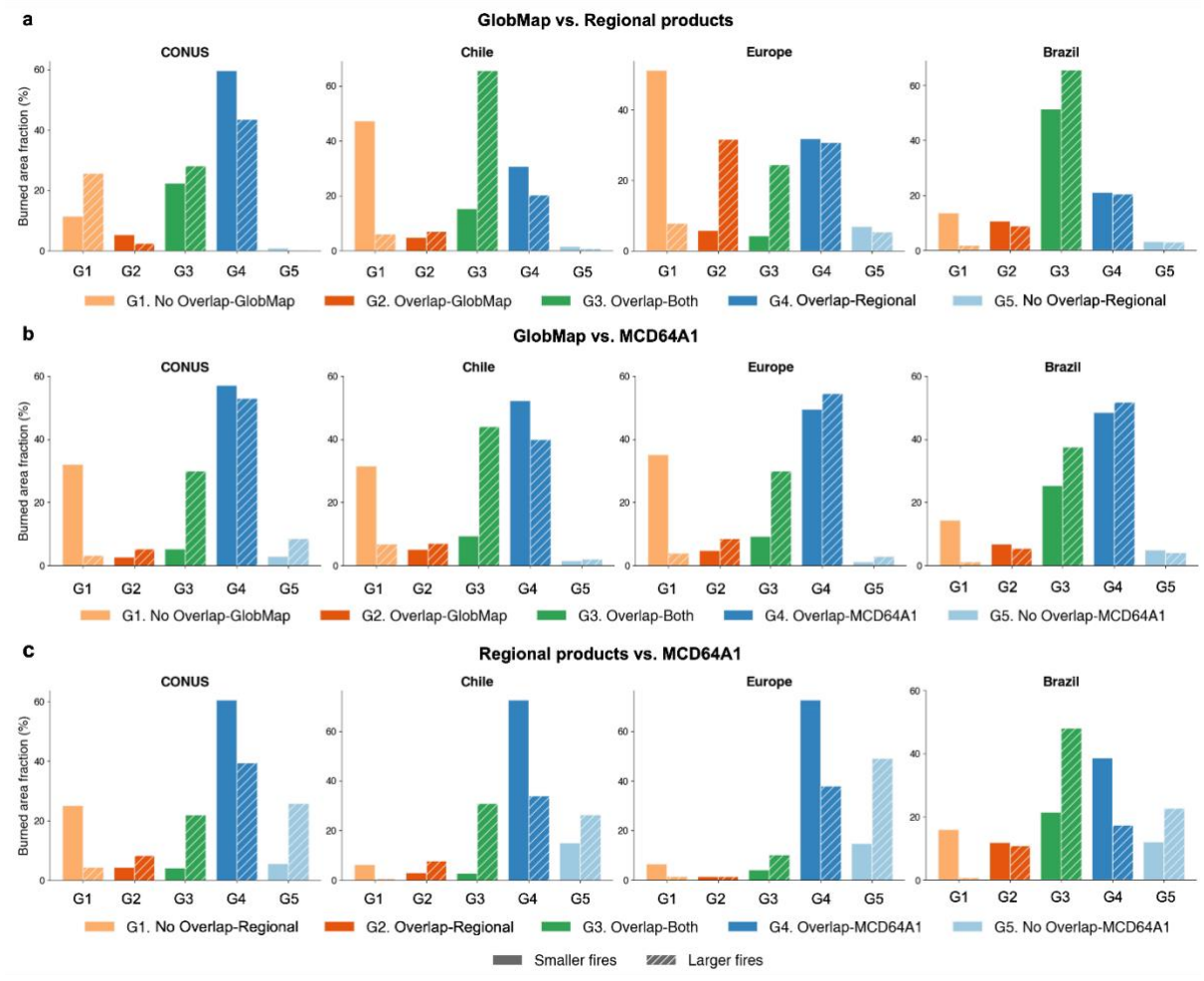

Figure 8. Spatial agreement patterns among Landsat-based products (GlobMap and existing regional products) and MCD64A1 across four regions. (a) Comparison between GlobMap and regional products since the 1980s: BAECV in CONUS, LFSD in Chile, EFDM in Europe, and MapBiomas in Brazil. (b) Comparison between GlobMap and MCD64A1 after 2001 in the same four regions. (c) Comparison between regional products and MCD64A1 after 2001. Light orange, dark orange, green, dark blue, and light blue colors represent Groups 1 – 5 (Fig. 4). Bars with solid fills represent smaller fire patches, while those with diagonal patterns represent larger ones.

https://doi.org/10.5194/essd-2025-733
Preprint. Discussion started: 10 December 2025

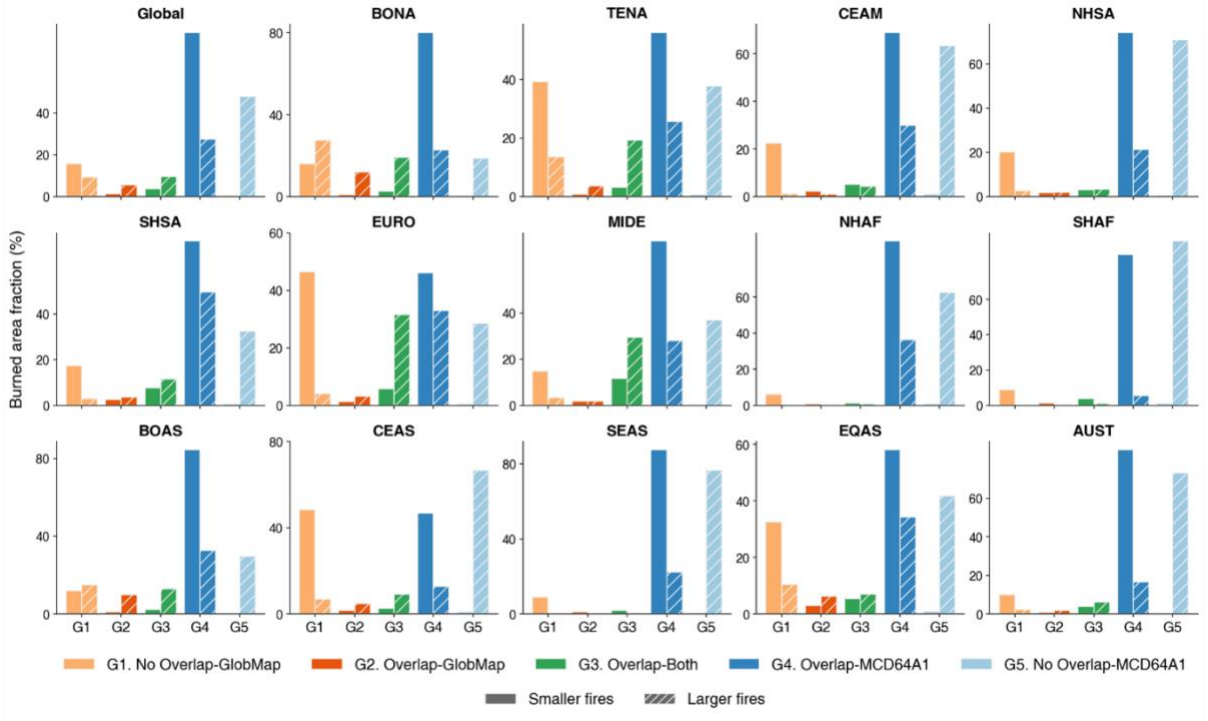

Figure 9. Spatial agreement patterns between GlobMap and MCD64A1 during 2001 and 2021 globally and across GFED regions. Light orange, dark orange, green, dark blue, and light blue colors represent Groups 1 – 5 (Fig. 4). Bars with solid fills represent smaller fire patches, while those with diagonal patterns represent larger ones.

4.3.3 Temporal agreement of detected burned year

Comparisons across products demonstrate the strong effectiveness of GlobMap in detecting the burned year of forest fires. Regionally, GlobMap generally exhibited better agreement with MCD64A1 after 2001 than the Landsat-based regional products, except in Europe (Fig. 10a-h). For both larger and smaller fire patches, GlobMap identified a higher fraction of samples detected within ± 3 years of MCD64A1. For example, in Chile, GlobMap achieved stronger temporal agreement (99.2% for larger fires and 60.0% for smaller fires) than LFSD (96.4% from and 59.5%, respectively) (Fig. 10b, f). Nevertheless, in Europe, GlobMap's agreement with MCD64A1 (81.3% for larger fires and 51.2% for smaller fires) was lower than that of EFDM (92.3% and 72.1%, respectively) (Fig. 10c, g). Further comparisons between GlobMap and existing Landsat-based regional products further confirmed their enhanced temporal consistency since the 1980s (Fig. 10i-l). In Chile, temporal agreement with LFSD was even stronger, with 99.5% and 81.4% of larger and smaller fires aligning within ± 3 years (Fig. 10j). In Europe, GlobMap aligned with EFDM for 83.6% of larger fire samples and 95.4% of smaller ones (Fig. 10k). In CONUS, GlobMap matched burned years within ± 3 years of BAECV for approximately 87.6% of larger fire samples and 79.0% of smaller ones (Fig. 10i). It is also worth noting that in Brazil's tropical forests, both the GlobMap and MapBiomas showed lower temporal agreement with MCD64A1 compared to other regions (Fig. 10d, h), highlighting the challenges of accurately detecting burned years in cloud-prone tropical ecosystems using Landsat data with lower observation frequency.

https://doi.org/10.5194/essd-2025-733
Preprint. Discussion started: 10 December 2025

Globally, the temporal agreement between GlobMap and MCD64A1 over 2001-2021 varies across regions and fire size groups. Burned years detected in boreal and temperate forests generally exhibited strong temporal agreement between the two products, with more than 85% of the samples showing year differences within ± 3 years in Boreal North America (BONA; 98.2%), Australia and New Zealand (AUST; 87.6%), Europe (EURO; 85.9%), Temperate North America (TENA; 85.8%), and Boreal Asia (BOAS; 85.0%; Fig. 11a). While fires in tropical forests generally showed lower performance in temporal agreement between the two products. Across all GFED regions, samples from larger fires (fire size exceeding 200 ha) tended to have better temporal agreement (Fig. 11b), with a higher proportion of fires detected within ± 3 years between the products than the smaller ones. The higher agreement for samples from larger fires was observed in forests of BONA (99.7%), AUST (97.2%), and TENA (95.7%), followed by those in EURO (94.1%), BOAS (91.2%), and Middle East (MIDE; 82.2%). In comparison, samples from smaller fires generally reached lower temporal agreement when compared to MCD64A1. The relative lower consistency in the tropics is likely due to the limited temporal resolution of Landsat observations in these regions, where persistent cloud cover and frequent repeated burnings could hinder the accurate detection of burned year. This also highlights the limitations of Landsat imagery in capturing fast-spread fires and rapidly recovering burned scars in grasslands and shrublands.

https://doi.org/10.5194/essd-2025-733
Preprint. Discussion started: 10 December 2025

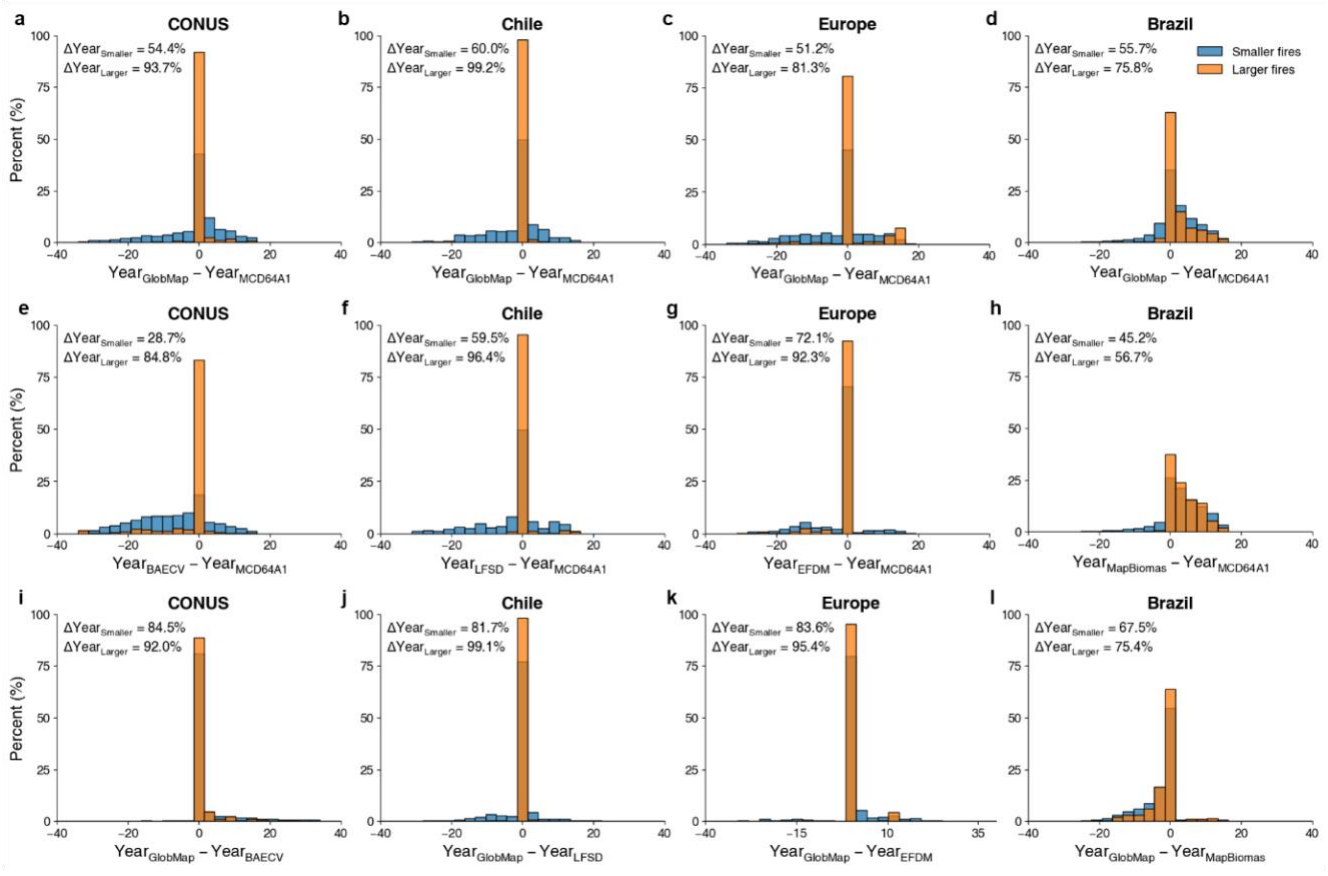

Figure 10. Histograms of burned year differences between Landsat-based products and MCD64A1. (a-d) Comparisons between GlobMap and MCD64A1 after 2001 in CONUS (a), Chile (b), Europe (c), and Brazil (d). (e-h) Comparisons between existing regional products and MCD64A1 in the same regions after 2001: BAECV in CONUS (e), LFSD in Chile (f), EFDM in Europe (g), and MapBiomas in Brazil (h). (i-l) Long-term comparisons between GlobMap and the regional products since the 1980s: CONUS (i), Chile (j), Europe (k), and Brazil (l). For each subplot, the percentages of samples with burned year differences within ± 3 years are displayed in the upper left corner, separately for smaller (< 200 ha, orange bars) and larger (≥ 200 ha, blue bars) fire size groups.

https://doi.org/10.5194/essd-2025-733
Preprint. Discussion started: 10 December 2025

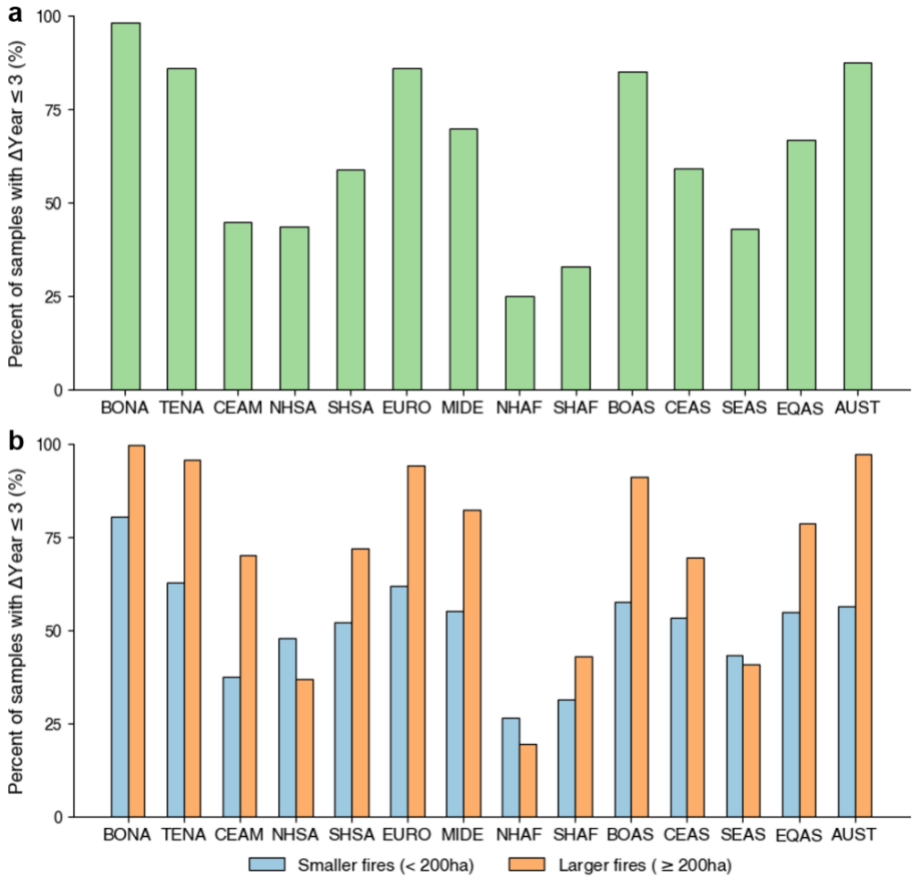

Figure 11. Fractions of fire patches with burned year differences within ± 3 years between the GlobMap and MCD64A1, summarized by GFED regions. (a) Overall agreement across all fire patches. (b) Fractions summarized by smaller (< 200 ha, orange bars) and larger fires (≥ 200 ha, blue bars) separately.

5 Discussions and conclusions

This study presents a 30 m global dataset of annual forest fire patches from 1984 to 2022, derived from Landsat imagery. This nearly four-decade record addresses a critical gap by providing a globally consistent, of individual forest fire patches with detailed spatial characterization. This product offers a foundation for analyzing long-term fire impacts and spatiotemporal shifts in forest fire regimes. By tracking patch-level characteristics consistently through time, it enables quantitative assessments of changes in fire frequency, fire size distributions, burned area contributions, and spatiotemporal aggregation of fire patches, within and across forest biomes. Because we constructed fire patches annually based on their burned years in the spatiotemporal clustering procedure, as limited by Landsat's coarse temporal resolution, fires occurring at different times within the same year but in close spatial proximity may be merged into a single patch. This may lead to overestimated patch sizes and underestimated fire frequencies, and should be considered when interpreting derived fire regime metrics. Another

https://doi.org/10.5194/essd-2025-733
Preprint. Discussion started: 10 December 2025

advantage of Landsat over MODIS-based products or management inventories is its improved ability to delineate actual burned area while retaining unburned refugia within fire perimeters (Fig. 12). This yields more accurate spatial representations of fire patches, but often with smaller size estimates than coarser datasets. For instance, in CONUS forests, the BAECV data maps smaller burned extent than the polygons delineated by the Monitoring Trends in Burn Severity (MTBS) product (Hawbaker et al., 2020). Similarly, in Chile, the LSFD identifies smaller fire sizes than those recorded by management records from the Chilean Forest Service (Miranda et al., 2022). Improved characterization of within-fire ecological refugia is especially crucial for conserving local biodiversity and ecosystem functioning, given continuing rise in fire risks across global forests under a warming climate (Meddens et al., 2016).

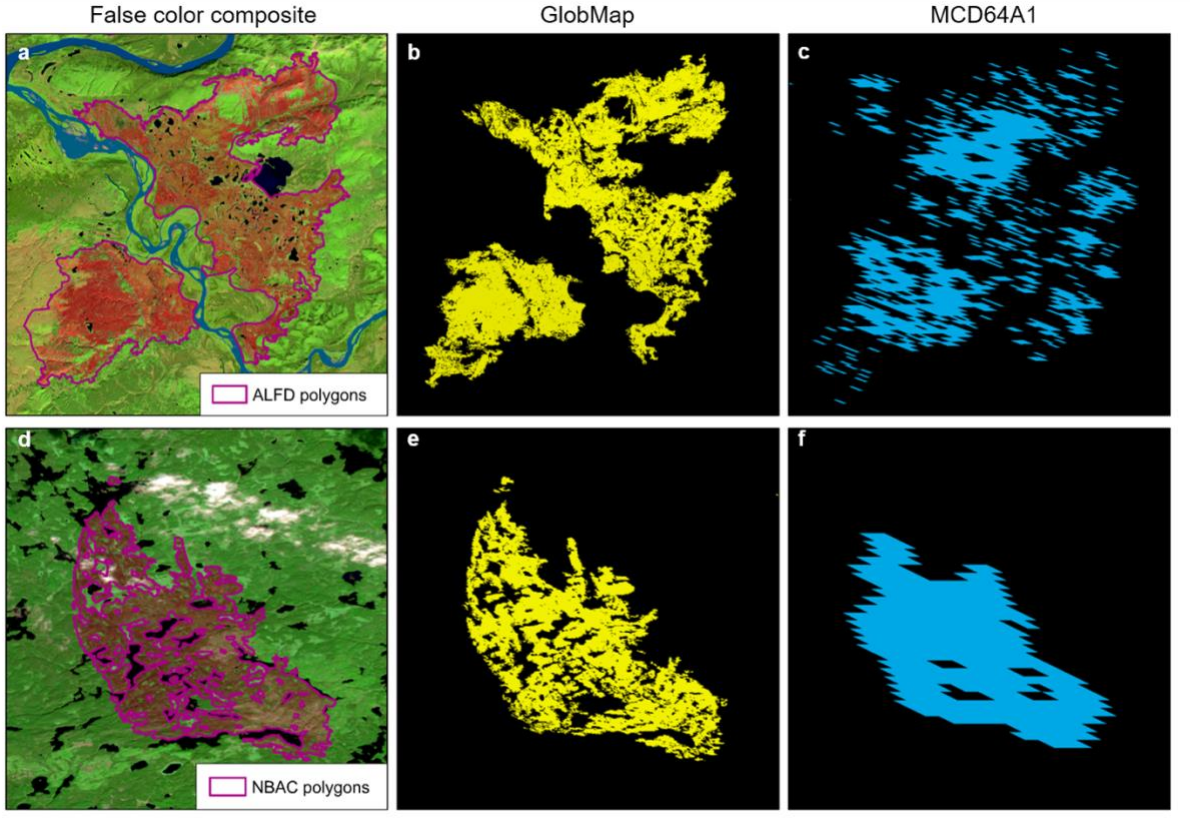

Figure 12. Examples of GlobMap mapping results and comparisons with false color composites, fire management polygons, and MCD64A1 at two forest sites. (a-c) Alaska, US: (a) false color composite of Landsat imagery from September 1, 2015, overlaid with polygons from the Alaska Large Fire Database (ALFD); (b) GlobMap results; (c) MCD64A1 results. (d-f) Eastern Canada: (d) false color composite of Landsat imagery from October 26, 2019, overlaid with polygons from the National Burned Area Composite database (NBAC); (e) GlobMap results; (f) MCD64A1 results.

Our minimum BVI method, combined with multi-year compositing, offers an efficient and robust strategy for generating clean, temporally consistent Landsat composites in large-scale burned area mapping. The minimum BVI method isolates true burned spectral signals without relying on imperfect cloud and shadow masks, yielding composites that more reliably capture surface changes with minimal residual contamination. It also reduces noise from missing pixels and scanlines in early Landsat 5 TM

https://doi.org/10.5194/essd-2025-733
Preprint. Discussion started: 10 December 2025

and Landsat 7 ETM+ imagery (Tucker et al., 2004), which can distort spectral signals and inflate burned area estimates. Coupled with multi-year compositing, this approach lowers computational demands on cloud platforms such as GEE, enabling efficient large-scale mapping with moderate- to high-resolution imagery. Given the rapid expansion of Earth observation archives, computationally streamlined methods are increasingly essential, as overly complex workflows can strain computing resources and increase energy consumption. By leveraging GEE's built-in data storage and processing capacity, our approach avoids local handling of massive datasets and greatly simplifies the processing pipeline. While the multi-year compositing strategy may underestimate burned area in forests with frequency surface fires, it effectively prevents repeated detection of persistent high-severity fire scars remaining visible for years in satellite imagery (Zhao et al., 2016; Boothman and Cardille, 2022; Gerard et al., 2003). It also mitigates temporal comparability issues arising from sparse and uneven coverage of early Landsat data in time-series analyses(Qiu et al., 2019), supporting a more consistent and reliable perception of long-term fire patterns. Thus, selecting an appropriate compositing window requires balancing temporal stability against preserving short-term ecological variability.

Mapping global forest fires with Landsat imagery also induces several limitations. First, the coarse temporal resolution of cloud-free Landsat observations constrains the temporal accuracy of burned area detection. With a 16-day revisit cycle, Landsat may miss fast-recovering surface fires, whose spectral signals could disappear before the next overpass (Hislop et al., 2018). Although Landsat generally provides reliable annual burn identification in most forests, where fires predominantly occur during relatively cloud-free dry seasons, its effectiveness substantially diminishes in persistently cloudy regions. This issue is particularly pronounced in moist tropical forests, where frequent cloud coverage reduces the effective temporal resolution and hinders precise estimation of burning dates. Second, restricted spatial coverage during the early Landsat era may result in underestimation of burned area. In regions such as Western and Central Africa and boreal Eurasia, Landsat acquisitions before the 2000s were sparse due to limited data acquisition strategy (e.g. storage constraints) and inconsistent ground-station reception and archiving (Feng and Wang, 2024). Nevertheless, in boreal forests, where post-fire tree recovery is often slow, particularly after severe stand-replacing fires, evidence of early burnings can still be detected despite incomplete archive. Additionally, fire type and intensity affect the detectability of burned area in optical imagery. Stand-replacing crown and high-intensity understory fires produce strong spectral signals and are typically well captured, whereas low-intensity understory burns and nighttime fires generate subtle or short-lived signals that may be omitted due to their spectral characteristics and fuel properties. Overall, these limitations highlight the need to combine Landsat with complementary high-frequency optical data (e.g., Sentinel-2) or all-weather sensors (e.g., SAR) to improve both the spatial and temporal completeness of global forest fire mapping.

These Landsat-specific limitations also explain differences between our dataset and MODIS-based products. MODIS's coarse spatial resolution integrates signals across large pixels, causing burned-area spectral changes to be detected even when only a fraction of the pixel is affected (Robinson, 1991). This spatial aggregation often produces larger, more spatially continuous burned perimeters and reduces the ability to resolve small or fine-scale fire features. In contrast, Landsat's 30 m resolution preserves within-fire heterogeneity and unburned refugia, yielding more spatially constrained patch boundaries. Discrepancies

https://doi.org/10.5194/essd-2025-733
Preprint. Discussion started: 10 December 2025

in detected burned years, particularly in tropical forests, are largely attributable to differences in temporal resolution between MODIS and Landsat. Tropical forests, unlike temperate and boreal forests, often experience persistent cloud cover and rapid vegetation regrowth after burning, causing fire signals to be frequently missed by cloud-free Landsat observations with a >16-day revisit cycle. MODIS, with its high-frequency observations, is more likely to capture these short-lived fire signatures, leading to earlier or more accurate burn-year assignments in cloudy tropical areas.

In summary, this study developed a new global forest fire dataset that maps individual fire patches at a 30 m spatial resolution over the past four decades. The pixel-based multi-temporal image compositing method adopted in this study is efficient for large-scale forest fire mapping on cloud computing platform such as the GEE. Comparisons with existing global and regional products suggest the effectiveness of this product in capturing the spatial extent and burned year of forest fires. This dataset shows great potential for quantifying historical fire regimes and assessing their ecological impacts across global forests over the long term. It also provides a critical data source for modeling and projecting future fire activity under climate warming.

6 Data availability

GlobMap FFP Dataset (version 1.0) is publicly available on Zenodo at https://doi.org/10.5281/zenodo.17638167 (Liu, 2025). The dataset is organized into seven ".zip" packages corresponding to compositing periods and is provide in 5°×5° Sinusoidal grid tiles (666 tiles in global forests). Each 30 m tile (18,533 × 18,533 pixels) includes three raster-format GeoTIFF files: (1) fire patch ID, (2) burned year, and (3) QA level. Files follow the naming convention: "ScarID_ScarTM3DV03_GEEScarTMSinv02_Clean.A3000001.h[HH]v[VV].[FILE_TYPE].[PERIOD].tif", where [HH] and [VV] denote the horizontal and vertical tile indices. [FILE_TYPE] corresponds to one of the three file types: "ScarID", "ScarYear", and "QualityFlag", representing fire patch ID, burned year, and QA level, respectively. The actual year of fire is obtained by adding 1980 to "ScarYear". Only QA levels 1 and 2 are included in the distributed dataset.

7 Author contributions

RL designed the algorithm, developed the software, generated the product, and performed the validation. JH conducted the product intercomparison and drafted the original manuscript. XZ and WZ conducted the image compositing workflow. QD supported the validation. All authors reviewed the final paper.

8 Competing interests

The contact author has declared that none of the authors has any competing interests.

https://doi.org/10.5194/essd-2025-733
Preprint. Discussion started: 10 December 2025

Open Access Earth System Science Data Discussions

9 Acknowledgement

This work was supported by the National Natural Science Foundation of China (Grant No. 42161144001).

References

Alencar, A. A. C., Arruda, V. L. S., Silva, W. V. d., Conciani, D. E., Costa, D. P., Crusco, N., Duverger, S. G., Ferreira, N. C., Franca-Rocha, W., Hasenack, H., Martenexen, L. F. M., Piontekowski, V. J., Ribeiro, N. V., Rosa, E. R., Rosa, M. R., dos Santos, S. M. B., Shimbo, J. Z., and Vélez-Martin, E.: Long-Term Landsat-Based Monthly Burned Area Dataset for the Brazilian Biomes Using Deep Learning, Remote Sensing, 14, 2510, 2022.

Andela, N., Morton, D. C., Giglio, L., Paugam, R., Chen, Y., Hantson, S., van der Werf, G. R., and Randerson, J. T.: The Global Fire Atlas of individual fire size, duration, speed, and direction, Earth System Science Data, 11, 529-552, 10.5194/essd-2018-89, 2019.

Archibald, S., Lehmann, C. E. R., Gómez-Dans, J. L., and Bradstock, R. A.: Defining pyromes and global syndromes of fire regimes, Proceedings of the National Academy of Sciences, 110, 6442-6447, 2013.

Artés, T., Oom, D., de Rigo, D., Durrant, T. H., Maianti, P., Libertà, G., and San-Miguel-Ayanz, J.: A global wildfire dataset for the analysis of fire regimes and fire behaviour, Scientific Data, 6, 296, 10.1038/s41597-019-0312-2, 2019.

Balch, J. K., St. Denis, L. A., Mahood, A. L., Mietkiewicz, N. P., Williams, T. M., McGlinchy, J., and Cook, M. C.: FIRED (Fire Events Delineation): An Open, Flexible Algorithm and Database of US Fire Events Derived from the MODIS Burned Area Product (2001–2019), Remote Sensing, 12, 3498, 2020.

Balch, J. K., Abatzoglou, J. T., Joseph, M. B., Koontz, M. J., Mahood, A. L., McGlinchy, J., Cattau, M. E., and Williams, A. P.: Warming weakens the night-time barrier to global fire, Nature, 602, 442-448, 10.1038/s41586-021-04325-1, 2022.

Barbosa, P. M., Pereira, J. M. C., and Grégoire, J.-M.: Compositing Criteria for Burned Area Assessment Using Multitemporal Low Resolution Satellite Data, Remote Sensing of Environment, 65, 38-49, https://doi.org/10.1016/S0034-4257(98)00016-9, 1998.

Beck, H. E., McVicar, T. R., Vergopolan, N., Berg, A., Lutsko, N. J., Dufour, A., Zeng, Z., Jiang, X., van Dijk, A. I. J. M., and Miralles, D. G.: High-resolution (1 km) Köppen-Geiger maps for 1901–2099 based on constrained CMIP6 projections, Scientific Data, 10, 724, 10.1038/s41597-023-02549-6, 2023.

Beck, P. S. A., Goetz, S. J., Mack, M. C., Alexander, H. D., Jin, Y., Randerson, J. T., and Loranty, M. M.: The impacts and implications of an intensifying fire regime on Alaskan boreal forest composition and albedo, Global Change Biology, 17, 2853-2866, 10.1111/j.1365-2486.2011.02412.x, 2011.

Boothman, R. and Cardille, J. A.: New techniques for old fires: Using deep learning to augment fire maps from the early satellite era, Frontiers in Environmental Science, Volume 10 - 2022, 10.3389/fenvs.2022.914493, 2022.

Brando, P. M., Silvério, D., Maracahipes-Santos, L., Oliveira-Santos, C., Levick, S. R., Coe, M. T., Migliavacca, M., Balch, J. K., Macedo, M. N., Nepstad, D. C., Maracahipes, L., Davidson, E., Asner, G., Kolle, O., and Trumbore, S.: Prolonged tropical forest degradation due to compounding disturbances: Implications for CO2 and H2O fluxes, Global Change Biology, 25, 2855-2868, https://doi.org/10.1111/gcb.14659, 2019.

Broich, M., Hansen, M. C., Potapov, P., Adusei, B., Lindquist, E., and Stehman, S. V.: Time-series analysis of multi-resolution optical imagery for quantifying forest cover loss in Sumatra and Kalimantan, Indonesia, International Journal of Applied Earth Observation and Geoinformation, 13, 277-291, https://doi.org/10.1016/j.jag.2010.11.004, 2011.

Chuvieco, E., Ventura, G., Martín, M. P., and Gómez, I.: Assessment of multitemporal compositing techniques of MODIS and AVHRR images for burned land mapping, Remote Sensing of Environment, 94, 450-462, https://doi.org/10.1016/j.rse.2004.11.006, 2005.

Chuvieco, E., Lizundia-Loiola, J., Lucrecia Pettinari, M., Ramo, R., Padilla, M., Tansey, K., Mouillot, F., Laurent, P., Storm, T., Heil, A., and Plummer, S.: Generation and analysis of a new global burned area product based on MODIS 250 m reflectance bands and thermal anomalies, Earth System Science Data, 10, 2015-2031, 10.5194/essd-10-2015-2018, 2018.

Chuvieco, E., Mouillot, F., van der Werf, G. R., San Miguel, J., Tanasse, M., Koutsias, N., García, M., Yebra, M., Padilla, M., Gitas, I., Heil, A., Hawbaker, T. J., and Giglio, L.: Historical background and current developments for mapping burned area from satellite Earth observation, Remote Sensing of Environment, 225, 45-64, 10.1016/j.rse.2019.02.013, 2019.

https://doi.org/10.5194/essd-2025-733
Preprint. Discussion started: 10 December 2025

Duan, Q., Liu, R., Chen, J., Wei, X., Liu, Y., and Zou, X.: Burned area detection from a single satellite image using an adaptive thresholds algorithm, International Journal of Digital Earth, 17, 2376275, 10.1080/17538947.2024.2376275, 2024.

Feng, L. and Wang, X.: Quantifying Cloud-free Observations from Landsat Missions: Implications for Water Environment Analysis, Journal of Remote Sensing, 4, 0110, 10.34133/remotesensing.0110, 2024.

Francini, S., Hermosilla, T., Coops, N. C., Wulder, M. A., White, J. C., and Chirici, G.: An assessment approach for pixel-based image composites, ISPRS Journal of Photogrammetry and Remote Sensing, 202, 1-12, https://doi.org/10.1016/j.isprsjprs.2023.06.002, 2023.

Franquesa, M., Vanderhoof, M. K., Stavrakoudis, D., Gitas, I. Z., Roteta, E., Padilla, M., and Chuvieco, E.: Development of a standard database of reference sites for validating global burned area products, Earth Syst. Sci. Data, 12, 3229-3246, 10.5194/essd-12-3229-2020, 2020.

Gerard, F., Plummer, S., Wadsworth, R., Ferreruela Sanfeliu, A., Iliffe, L., Balzter, H., and Wyatt, B.: Forest fire scar detection in the boreal forest with multitemporal SPOT-VEGETATION data, IEEE Transactions on Geoscience and Remote Sensing, 41, 2575-2585, 10.1109/TGRS.2003.819190, 2003.

Giglio, L., Boschetti, L., Roy, D. P., Humber, M. L., and Justice, C. O.: The Collection 6 MODIS burned area mapping algorithm and product, Remote Sensing of Environment, 217, 72-85, https://doi.org/10.1016/j.rse.2018.08.005, 2018.

Hansen, M. C., Potapov, P. V., Moore, R., Hancher, M., Turubanova, S. A., Tyukavina, A., Thau, D., Stehman, S. V., Goetz, S. J., Loveland, T. R., Kommareddy, A., Egorov, A., Chini, L., Justice, C. O., and Townshend, J. R. G.: High-Resolution Global Maps of 21st-Century Forest Cover Change, Science, 342, 850-854, 10.1126/science.1244693, 2013.

Hantson, S., Pueyo, S., and Chuvieco, E.: Global fire size distribution is driven by human impact and climate, Global Ecology and Biogeography, 24, 77-86, https://doi.org/10.1111/geb.12246, 2015.

Hawbaker, T. J., Vanderhoof, M. K., Schmidt, G. L., Beal, Y. J., Picotte, J. J., Takacs, J. D., Falgout, J. T., and Dwyer, J. L.: The Landsat Burned Area algorithm and products for the conterminous United States, Remote Sensing of Environment, 244, 111801, 10.1016/j.rse.2020.111801, 2020.

Hermosilla, T., Wulder, M. A., White, J. C., and Coops, N. C.: Prevalence of multiple forest disturbances and impact on vegetation regrowth from interannual Landsat time series (1985–2015), Remote Sensing of Environment, 233, 111403, https://doi.org/10.1016/j.rse.2019.111403, 2019.

Hislop, S., Jones, S., Soto-Berelov, M., Skidmore, A., Haywood, A., and Nguyen, T. H.: Using Landsat Spectral Indices in Time-Series to Assess Wildfire Disturbance and Recovery, Remote Sensing, 10, 460, 2018.

Huang, C., Goward, S. N., Masek, J. G., Thomas, N., Zhu, Z., and Vogelmann, J. E.: An automated approach for reconstructing recent forest disturbance history using dense Landsat time series stacks, Remote Sensing of Environment, 114, 183-198, https://doi.org/10.1016/j.rse.2009.08.017, 2010.

Iglesias, V., Balch, J. K., and Travis, W. R.: U.S. fires became larger, more frequent, and more widespread in the 2000s, Science Advances, 8, eabc0020, 10.1126/sciadv.abc0020, 2022.

Kennedy, R. E., Yang, Z., and Cohen, W. B.: Detecting trends in forest disturbance and recovery using yearly Landsat time series: 1. LandTrendr — Temporal segmentation algorithms, Remote Sensing of Environment, 114, 2897-2910, https://doi.org/10.1016/j.rse.2010.07.008, 2010.

Liu, R.: Compositing the Minimum NDVI for MODIS Data, IEEE Transactions on Geoscience and Remote Sensing, 55, 1396-1406, 10.1109/TGRS.2016.2623746, 2017.

Liu, R.: A Global 30 m Landsat-based Dataset of Forest Fire Patches (GlobMap FFP v1.0) from 1984 to 2022, Zenodo [dataset], https://doi.org/10.5281/zenodo.17638167, 2025.

Liu, Y., Liu, R., Chen, J., Wei, X., Qi, L., and Zhao, L.: A global annual fractional tree cover dataset during 2000–2021 generated from realigned MODIS seasonal data, Scientific Data, 11, 832, 10.1038/s41597-024-03671-9, 2024.

Liu, Z., Ballantyne, A. P., and Cooper, L. A.: Biophysical feedback of global forest fires on surface temperature, Nature Communications, 10, 1-9, 10.1038/s41467-018-08237-z, 2019.

Long, T., Zhang, Z., He, G., Jiao, W., Tang, C., Wu, B., Zhang, X., Wang, G., and Yin, R.: 30 m Resolution Global Annual Burned Area Mapping Based on Landsat Images and Google Earth Engine, Remote Sensing, 11, 489, 2019.

Lv, Q., Chen, Z., Wu, C., Peñuelas, J., Fan, L., Su, Y., Yang, Z., Li, M., Gao, B., Hu, J., Zhang, C., Fu, Y., and Wang, Q.: Increasing severity of large-scale fires prolongs recovery time of forests globally since 2001, Nature Ecology & Evolution, 9, 980-992, 10.1038/s41559-025-02683-x, 2025.

https://doi.org/10.5194/essd-2025-733
Preprint. Discussion started: 10 December 2025

Meddens, A. J. H., Kolden, C. A., and Lutz, J. A.: Detecting unburned areas within wildfire perimeters using Landsat and ancillary data across the northwestern United States, Remote Sensing of Environment, 186, 275-285, https://doi.org/10.1016/j.rse.2016.08.023, 2016.

Miettinen, J. and Liew, S. C.: Comparison of multitemporal compositing methods for burnt area detection in Southeast Asian conditions, International Journal of Remote Sensing, 29, 1075-1092, 10.1080/01431160701281031, 2008.

Miranda, A., Mentler, R., Moletto-Lobos, Í., Alfaro, G., Aliaga, L., Balbontín, D., Barraza, M., Baumbach, S., Calderón, P., Cárdenas, F., Castillo, I., Contreras, G., de la Barra, F., Galleguillos, M., González, M. E., Hormazábal, C., Lara, A., Mancilla, I., Muñoz, F., Oyarce, C., Pantoja, F., Ramírez, R., and Urrutia, V.: The Landscape Fire Scars Database: mapping historical burned area and fire severity in Chile, Earth Syst. Sci. Data, 14, 3599-3613, 10.5194/essd-14-3599-2022, 2022.

Nair, V. and Hinton, G. E.: Rectified linear units improve restricted boltzmann machines, Proceedings of the 27th International Conference on International Conference on Machine Learning, Haifa, Israel2010.

Otón, G., Ramo, R., Lizundia-Loiola, J., and Chuvieco, E.: Global Detection of Long-Term (1982–2017) Burned Area with AVHRR-LTDR Data, 10.3390/rs11182079, 2019.

Padilla, M., Stehman, S. V., Ramo, R., Corti, D., Hantson, S., Oliva, P., Alonso-Canas, I., Bradley, A. V., Tansey, K., Mota, B., Pereira, J. M., and Chuvieco, E.: Comparing the accuracies of remote sensing global burned area products using stratified random sampling and estimation, Remote Sensing of Environment, 160, 114-121, https://doi.org/10.1016/j.rse.2015.01.005, 2015.

Pugh, T. A. M., Arneth, A., Kautz, M., Poulter, B., and Smith, B.: Important role of forest disturbances in the global biomass turnover and carbon sinks, Nature Geoscience, 12, 730-735, 10.1038/s41561-019-0427-2, 2019.

Qiu, S., Zhu, Z., Olofsson, P., Woodcock, C. E., and Jin, S.: Evaluation of Landsat image compositing algorithms, Remote Sensing of Environment, 285, 113375, https://doi.org/10.1016/j.rse.2022.113375, 2023.

Qiu, S., Lin, Y., Shang, R., Zhang, J., Ma, L., and Zhu, Z.: Making Landsat Time Series Consistent: Evaluating and Improving Landsat Analysis Ready Data, 10.3390/rs11010051, 2019.

Ramo, R., Roteta, E., Bistinas, I., van Wees, D., Bastarrika, A., Chuvieco, E., and van der Werf, G. R.: African burned area and fire carbon emissions are strongly impacted by small fires undetected by coarse resolution satellite data, Proceedings of the National Academy of Sciences of the United States of America, 118, 1-7, 10.1073/pnas.2011160118, 2021.

Robinson, J. M.: Fire from space: Global fire evaluation using infrared remote sensing, International Journal of Remote Sensing, 12, 3-24, 10.1080/01431169108929628, 1991.

Roteta, E., Bastarrika, A., Padilla, M., Storm, T., and Chuvieco, E.: Development of a Sentinel-2 burned area algorithm : Generation of a small fire database for sub-Saharan Africa, Remote Sensing of Environment, 222, 1-17, 10.1016/j.rse.2018.12.011, 2019.

Scholten, R. C., Coumou, D., Luo, F., and Veraverbeke, S.: Early snowmelt and polar jet dynamics co-influence recent extreme Siberian fire seasons, Science, 378, 1005-1009, 10.1126/science.abn4419, 2022.

Senf, C. and Seidl, R.: Mapping the forest disturbance regimes of Europe, Nature Sustainability, 4, 63-70, 10.1038/s41893-020-00609-y, 2021a.

Senf, C. and Seidl, R.: Storm and fire disturbances in Europe: Distribution and trends, Global Change Biology, 27, 3605-3619, https://doi.org/10.1111/gcb.15679, 2021b.

Sulla-Menashe, D., Gray, J. M., Abercrombie, S. P., and Friedl, M. A.: Hierarchical mapping of annual global land cover 2001 to present: The MODIS Collection 6 Land Cover product, Remote Sensing of Environment, 222, 183-194, https://doi.org/10.1016/j.rse.2018.12.013, 2019.

Tuccella, P., Di Antonio, L., Di Muzio, A., Colaiuda, V., Lidori, R., Menut, L., Pitari, G., and Raparelli, E.: Modeling the Black and Brown Carbon Absorption and Their Radiative Impact: The June 2023 Intense Canadian Boreal Wildfires Case Study, Journal of Geophysical Research: Atmospheres, 130, e2024JD042674, https://doi.org/10.1029/2024JD042674, 2025.

Tucker, C. J., Grant, D. M., and Dykstra, J. D.: NASA's global orthorectified Landsat data set, Photogrammetric Engineering & Remote Sensing, 70, 313-322, 2004.

Tyukavina, A., Potapov, P., Hansen, M. C., Pickens, A. H., Stehman, S. V., Turubanova, S., Parker, D., Zalles, V., Lima, A., Kommareddy, I., Song, X.-P., Wang, L., and Harris, N.: Global Trends of Forest Loss Due to Fire From 2001 to 2019, Frontiers in Remote Sensing, 3, 10.3389/frsen.2022.825190, 2022.

van Wees, D., van der Werf, G. R., Randerson, J. T., Andela, N., Chen, Y., and Morton, D. C.: The role of fire in global forest loss dynamics, Global Change Biology, 27, 2377-2391, https://doi.org/10.1111/gcb.15591, 2021.

https://doi.org/10.5194/essd-2025-733
Preprint. Discussion started: 10 December 2025

Veraverbeke, S., Rogers, B. M., Goulden, M. L., Jandt, R. R., Miller, C. E., Wiggins, E. B., and Randerson, J. T.: Lightning as a major driver of recent large fire years in North American boreal forests, Nature Clim. Change, 7, 529-534, 10.1038/nclimate3329, 2017.

White, J. C., Wulder, M. A., Hobart, G. W., Luther, J. E., Hermosilla, T., Griffiths, P., Coops, N. C., Hall, R. J., Hostert, P., Dyk, A., and Guindon, L.: Pixel-Based Image Compositing for Large-Area Dense Time Series Applications and Science, Canadian Journal of Remote Sensing, 40, 192-212, 10.1080/07038992.2014.945827, 2014.

Zhao, F. R., Meng, R., Huang, C., Zhao, M., Zhao, F. A., Gong, P., Yu, L., and Zhu, Z.: Long-Term Post-Disturbance Forest Recovery in the Greater Yellowstone Ecosystem Analyzed Using Landsat Time Series Stack, Remote Sensing, 8, 898, 2016.

Zheng, B., Ciais, P., Chevallier, F., Chuvieco, E., Chen, Y., and Yang, H.: Increasing forest fire emissions despite the decline in global burned area, Science Advances, 7, eabh2646, 10.1126/sciadv.abh2646, 2021.